Aharonov-Bohm oscillations in phosphorene quantum rings

L. L. Li,[1,2,*] D. Moldovan,[1,†] P. Vasilopoulos,[3,‡] and F. M. Peeters[1,§]

[1]*Department of Physics, University of Antwerp, Groenenborgerlaan 171, B-2020 Antwerpen, Belgium*

[2]*Key Laboratory of Materials Physics, Institute of Solid State Physics, Chinese Academy of Sciences, Hefei 230031, China*

[3]*Department of Physics, Concordia University, 7141 Sherbrooke West, Montreal, Quebec, Canada H4B 1R6*

(Received 27 February 2017; published 22 May 2017)

The Aharonov-Bohm (AB) effect in square phosphorene quantum rings, with armchair and zigzag edges, is investigated using the tight-binding method. The energy spectra and wave functions of such rings, obtained as a function of the magnetic flux Φ threading the ring, are strongly influenced by the ring width W, an in-plane electric field E_p, and a side-gating potential V_g. Compared to a square dot, the ring shows an enhanced confinement due to its inner edges and an interedge coupling along the zigzag direction, both of which strongly affect the energy spectrum and the wave functions. The energy spectrum that is gapped consists of a regular part, of conduction (valence) band states, that shows the usual AB oscillations in the higher- (lower-) energy region, and of edge states, in the gap, that exhibit no AB oscillations. As the width W decreases, the AB oscillations become more distinct and regular and their period is close to $\Phi_0/2$, where the flux quantum $\Phi_0 = h/e$ is the period of an ideal circular ring ($W \to 0$). Both the electric field E_p and the side-gating potential V_g reduce the amplitude of the AB oscillations. The amplitude can be effectively tuned by E_p or V_g and exhibits an anisotropic behavior for different field directions or side-gating configurations.

DOI: 10.1103/PhysRevB.95.205426

I. INTRODUCTION

Quantum confinement effects occur in low-dimensional systems and lead to strong modifications of the electronic, optical, and transport properties when compared with bulk systems. In this context, semiconductor nanostructures, such as quantum wells, wires, and dots, have been the subject of intense research interest [1]. Another important class of such low-dimensional systems are quantum rings [2], in which the phase coherence of the carrier wave function allows the observation of quantum interference effects such as the Aharonov-Bohm (AB) effect [3]. A remarkable property of quantum rings is that an equilibrium current, the so-called persistent current, can be driven by an external magnetic field without any external sources [4]. This is a direct consequence of the AB effect, which manifests itself in the energy spectrum of the ring as a periodic function of the magnetic flux threading the ring. The AB effect and persistent currents have been extensively studied in semiconductor quantum rings both experimentally [5–8] and theoretically [9–11], and are expected to have potential applications in quantum electronics and quantum information.

Nanoscale quantum rings have been fabricated from two-dimensional (2D) materials, in which the phase coherence length is larger than or comparable to their circumferences at low temperatures. This implies that the AB effect is observable in such rings. Actually, many experimental [12–15] and theoretical [16–22] studies of the AB effect in graphene quantum rings have been made but, to our knowledge, little on phosphorene quantum rings (PQRs).

Phosphorene, a relatively new 2D material, has recently been exfoliated [23,24]. Owing to its unique properties, it has attracted a lot of attention from the research community. Compared to other known 2D materials, such as graphene (having zero band gap) [25] and single-layer MoS_2 (having low carrier mobility) [26], phosphorene has the combined properties of a finite (direct) band gap [27] and a relatively high carrier mobility [23], which is crucial for practical applications such as field-effect transistors. Another striking property of phosphorene is its anisotropic optical response to linearly polarized light [28–30]. This property is not present in most other 2D materials, such as graphene and single-layer MoS_2, and makes phosphorene a natural candidate for optical devices that manipulate the light polarization.

Most recently, nanometer-sized phosphorene quantum dots (PQDs) have been fabricated and characterized [31,32]. This motivated theoretical studies of the electronic and optical properties of PQDs [33–35]. Some interesting results were obtained, such as unconventional edge states in PQDs [33,35] and anomalous size-dependent optical properties of PQDs [34]. Since a PQR can be viewed as a PQD containing an antidot, which introduces inner edges to the system, one can expect that the geometry of the ring and, depending on its width, the interedge coupling will lead to new physical properties which are not present in a PQD.

Previously, we investigated the electric and magnetic field dependence of the electronic and optical properties of PQDs by means of the tight-binding (TB) approach [35]. In the present paper, we will extend this approach to PQRs and study how the ring width, an in-plane electric field, and a side-gating potential influence the energy spectrum and the wave functions of a PQR. Compared to frequently employed continuum models, a major advantage of the TB model is that it takes into account the atomic structure of the ring that is particularly important for very narrow rings exhibiting edge states.

The main results obtained in this work are as follows: (i) The AB oscillation, observed in the energy spectrum of a PQR, depends strongly on the ring width, the in-plane electric field, and the side-gating potential, and (ii) the spectrum

*longlong.li@uantwerpen.be

†dean.moldovan@uantwerpen.be

‡p.vasilopoulos@concordia.ca

§francois.peeters@uantwerpen.be

contains edge states that are almost insensitive to the magnetic flux through the ring, which makes PQRs different from traditional quantum rings made of metals or semiconductors. We analyze and discuss these results using the wave-function properties of PQRs. There are mainly the following two reasons for studying phosphorene rings and not semiconductor or graphene rings in the present work: (i) Phosphorene rings support inner and outer edge states which are distinctly different than those in traditional semiconductor rings; and (ii) phosphorene rings exhibit highly anisotropic AB oscillations in their energy spectra, which are not present in graphene rings.

The paper is organized as follows. In Sec. II we present the TB model for a PQR subjected to a perpendicular magnetic field and to an in-plane electric field or a side-gating potential. In Sec. III we calculate the energy levels and the corresponding wave functions as a function of the magnetic flux threading the ring, and investigate the influences of the ring width, the electric field, and the side-gating potential. Finally, we make a summary and give concluding remarks in Sec. IV.

II. TIGHT-BINDING MODEL

We start with a square PQD (SPQD) of side length L [see Fig. 1(a)], a finite phosphorene lattice, using the TB model developed in Ref. [36]. The TB Hamiltonian is given by

$$H = \sum_i \varepsilon_i c_i^\dagger c_i + \sum_{i,j} t_{ij} c_i^\dagger c_j. \quad (1)$$

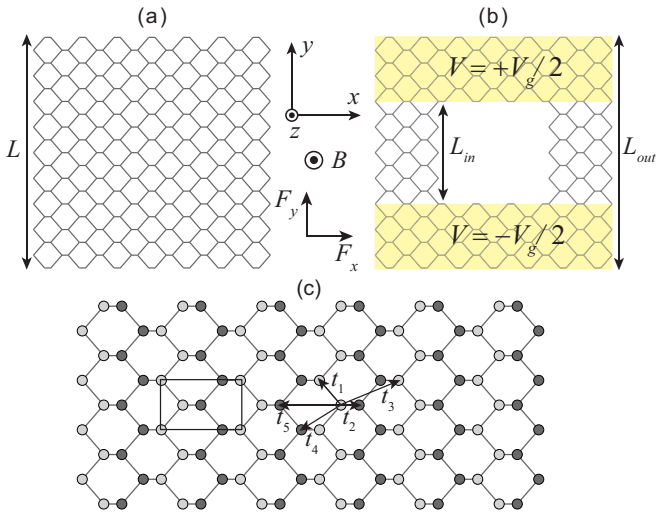

FIG. 1. Schematic view of (a) a SPQD and (b) a SPQR, with armchair edges along the x direction and zigzag edges along the y direction, in the presence of an external perpendicular magnetic field B. L is the side length of the SPQD, and $L_{\rm in}$ ($L_{\rm out}$) is the length of the inner (outer) side of the SPQR, so the ring width is given by $W = (L_{\rm out} - L_{\rm in})/2$. The entire SPQR may be subject to an in-plane electric field, F_x or F_y, or have different side-gating potentials $\pm V_g/2$ applied to its arms (indicated by the yellow regions). (c) Schematic lattice structure of phosphorene (top view). The unit cell (rectangle) consists of four inequivalent phosphorus atoms with two of them labeled by dark-gray solid circles and the other two labeled by light-gray solid circles. The symbols t_1–t_5 denote five hopping links between different phosphorus atoms.

The summation runs over all lattice sites of the system, ε_i is the on-site energy at site i, t_{ij} is the hopping energy between sites i and j, and $c_i^\dagger$ (c_j) is the creation (annihilation) operator of an electron at site i (j). It has been shown [36] that it is sufficient to take five hopping energies to describe the band structure of phosphorene, namely, $t_1 = -1.220$ eV, $t_2 = 3.665$ eV, $t_3 = -0.205$ eV, $t_4 = -0.105$ eV, and $t_5 = -0.055$ eV. In addition, the on-site energies are taken as $\varepsilon = 0$ for all lattice sites in the absence of external fields and potentials.

We identify the hopping matrix elements t_1–t_5 between different phosphorus atoms in Fig. 1(c). The above on-site energy and hopping energies are chosen such that the resulting TB model gives a good description of the phosphorene band structure, in the low-energy region near the band gap, as compared to density functional theory (DFT) calculations in the GW approximation (see Ref. [36]). This is done by using a truncation of the hopping energies and a reoptimization of the remaining parameters. Notice that there is only one orbital per atom in the TB model, because, according to DFT calculations [36], the p_z orbital has the largest contribution in both the conduction and valence bands in the low-energy region near the band gap. In the high-energy region, well above the band gap, the TB model needs to be modified by including more atomic orbitals such as the s, p_x, and p_y ones due to their large mixture with the p_z orbital (see Ref. [36] and also Ref. [37]). Inside a phosphorene layer, each atom is covalently bonded with three adjacent phosphorus atoms to form a puckered lattice structure due to the sp^3 hybridization. This structure can be viewed as consisting of two sublayers in which the bonding energy is dominated by the in-plane (intrasublayer) $pp\pi$ bonds and the out-of-plane (intersublayer) $pp\sigma$ bonds, with the latter much stronger than the former. The result is that t_2 has the largest magnitude, because it is derived from the strong out-of-plane σ-σ bonding between the p_z orbitals in the different sublayers, while t_1 and t_3 are derived from the relatively weak in-plane π-π bonding between the p_z orbitals in the same sublayer. Although t_4 and t_5 have the same derivation as t_2, their bonding distances are much larger and, as a result, their magnitudes are much smaller.

The TB model based on Eq. (1) has been applied previously to phosphorene nanoribbons [38] and PQDs [33,35]. Here, we extend it to PQRs in the presence of external fields and potentials. To create the ring geometry, a central region, empty of any atoms (antidot), is introduced in the original dot by setting the hopping parameters equal to zero for all absent atoms. We also remove all dangling bonds that are possibly present at the inner and outer edges.

In the present work we consider a square PQR (SPQR) with inner and outer side lengths $L_{\rm in}$ and $L_{\rm out}$ placed in the (x,y) plane, as shown in Fig. 1(b). Due to the same shape for the dot and antidot, the SPQR has armchair edges along the x direction and zigzag edges along the y direction at both the outer and inner boundaries. When an in-plane electric field F is applied to the SPQR along the armchair (zigzag) direction, the on-site energies in the TB Hamiltonian (1) should be modified by adding an electric potential term $-eF_x x$ ($-eF_y y$), with e being the electron charge. However, when a perpendicular magnetic field B is applied to the SPQR, the hopping energies

t_{ij} in Eq. (1) should be replaced by

$$t_{ij} \rightarrow t_{ij} \exp\left(i\frac{2\pi e}{h}\int_{\mathbf{r}_i}^{\mathbf{r}_j}\mathbf{A}\cdot d\mathbf{l}\right), \tag{2}$$

where h is Planck's constant and $\mathbf{A}$ the vector potential induced by the field B. We use the Landau gauge, and we have $\mathbf{A} = (0, Bx, 0)$. The magnetic flux threading the ring is defined as $\Phi = BS$ in units of the flux quantum $\Phi_0 = h/e$, where S is taken as the average area, $S = (S_{\text{in}} + S_{\text{out}})/2$, with S_{in} and S_{out} being the areas enclosed by the inner and outer edges of the ring, respectively.

We also take into account different side-gate potentials V_g applied to the upper and lower arms of the SPQR [see Fig. 1(b)] or to its left and right arms. Such potentials create an asymmetry between the two arms. In the present work we consider an asymmetric side-gating potential, which can be modeled as $V_{y(x)}(x,y) = V_g/2$ with $y > L_{\text{in}}/2$ ($x < -L_{\text{in}}/2$) for the upper (left) arm and $V_{y(x)}(x,y) = -V_g/2$ with $y < -L_{\text{in}}/2$ ($x > -L_{\text{in}}/2$) for the lower (right) arm, and this potential is added to the on-site energies in the TB Hamiltonian (1). Experimentally, the side-gating influence on the AB effect was previously studied in a circular graphene ring [13] with different finite voltages applied to its arms.

The energy levels and wave functions of the PQR are obtained by diagonalizing the TB Hamiltonian matrix numerically. All TB calculations are performed using the recently developed PYBINDING package [39].

III. RESULTS AND DISCUSSION

Below, we first present the energy spectrum of a square PQD (SPQD) as a function of the magnetic flux, that we use as a starting point, together with that for a ring of fixed width made out of this SPQD. Then we investigate the influence of varying the width on the spectrum of the ring, and finally that of an in-plane electric field and of a side-gating potential.

A. Quantum dot versus quantum ring

A SPQD with armchair and zigzag edges is schematically shown in Fig. 1(a). For the numerical calculation the dot side is taken $L = 8$ nm long. The energy spectrum as a function of the magnetic flux is plotted in Figs. 2(a)–2(d). To accentuate the magnetic field dependence, the energy-spectrum regions denoted by the three red rectangles shown in Fig. 2(a) are enlarged in Figs. 2(b)–2(d). As can be seen, the energy levels in the valence (conduction) band shown in Fig. 2(b) [Fig. 2(d)] correspond to the so-called bulk states, which are mainly distributed in the central region of the SPQD. These bulk levels approach the Landau levels (LLs) at high magnetic fields. The nearly flat energy levels in the band gap, shown in Fig. 2(c), correspond to the edge states, which are strongly localized at the zigzag boundaries of the SPQD. These edge states are almost unaffected by the magnetic field due to their strong localized nature. Here, we distinguish bulk and edge states according to their wave-function properties.

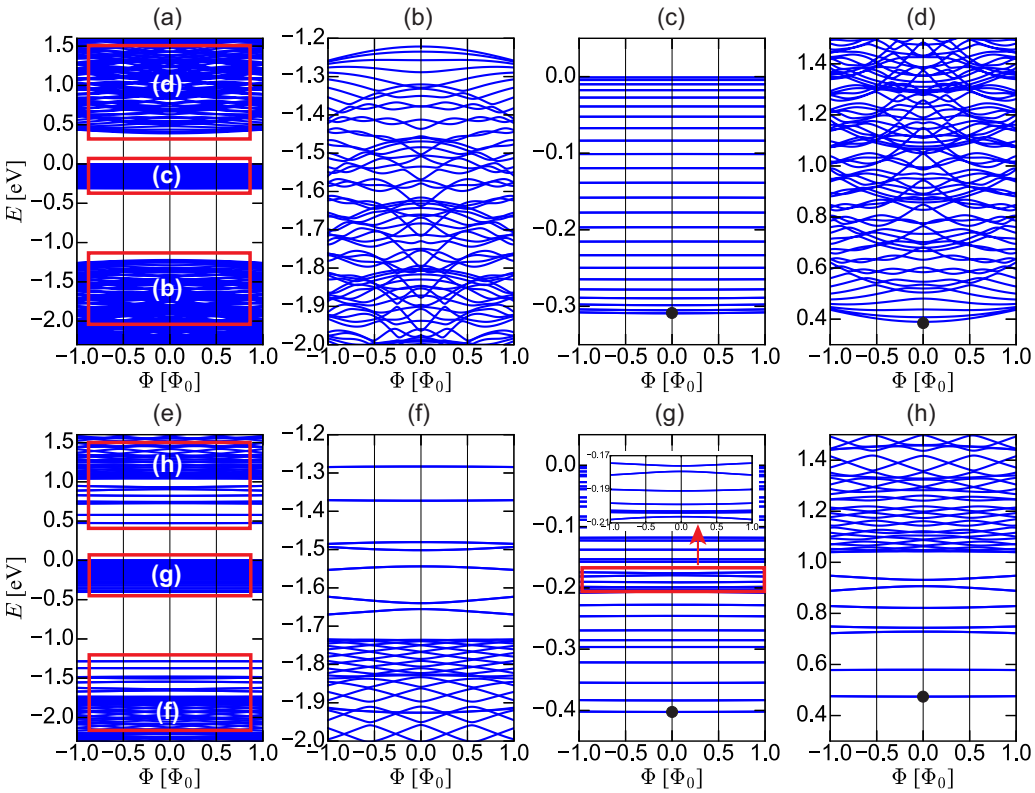

FIG. 2. (a)–(d) Energy spectrum of a SPQD, with side length $L = 8$ nm, as a function of the magnetic flux at zero electric field and side-gating potential. (e)–(h) As in (a)–(d) for a SPQR, with an outer (inner) side length $L_{\text{out}} = 8$ nm ($L_{\text{in}} = 4$ nm). Both the dot and the ring have armchair edges along the x direction and zigzag edges along the y direction. The red rectangles shown in (a) and (e) are enlarged next to them, as indicated, and that in (g) is enlarged in the inset.

We now contrast the energy spectrum of this SPQD with that of a SPQR that can be created by piercing a square hole (or square antidot) in the middle of the SPQD, as shown schematically in Fig. 1(b). This hole introduces inner edges to the original dot that are also armchair or zigzag type. In the numerical calculation the outer and inner side lengths are taken as $L_{\rm out} = 8$ nm and $L_{\rm in} = 4$ nm, respectively, so the ring width is $W = (L_{\rm out} - L_{\rm in})/2 = 2$ nm. Comparing Figs. 2(e)–2(h) with Figs. 2(a)–2(d), we observe the following differences: (1) The bulk levels have larger energy separations because of the enhanced confinement in the ring; (2) this enhanced confinement also renders the lowest (highest) bulk levels in the conduction (valence) band almost independent of the magnetic flux Φ; (3) the bulk levels in the higher- (lower-) energy range in the conduction (valence) band oscillate with Φ, that is, they exhibit the AB effect; (4) the number of edge states increases, compared to that for the dot, in a given energy range, as shown in Figs. 2(c) and 2(g); this is due to the increased number of zigzag edges in the ring since the edge states occur only at the zigzag edges; and (5) some edge-state levels shown in Fig. 2(g), e.g., those with energy between $E = -0.21$ and -0.17 eV, are not perfectly flat but vary slightly with Φ, as shown in its inset; this is due to a partial delocalization of those edge states induced by the interedge coupling in the ring.

To understand the origins of bulk and edge states, the enhanced confinement, and the interedge coupling mentioned above, we plot in Fig. 3 the probability densities of the lowest-energy states shown in Figs. 2(d) and 2(h) and of those shown in Figs. 2(c) and 2(g) all for zero magnetic flux ($\Phi = 0$) (they are indicated by the solid black dots in these figures). Here, (α) and (β) correspond to Figs. 2(d) and 2(h), respectively, showing the results for the SPQD, while (γ) and (δ) correspond to Figs. 2(c) and 2(g), respectively, showing those for the SPQR. These probability densities are normalized with respect to their maximum values. As can be seen, in both the SPQD and SPQR the bulk states are mainly distributed in the bulk parts (i.e., away from the boundaries) while the edge states are strongly localized at the zigzag boundaries. However, comparing Figs. 3(α) and 3(γ) as well as Figs. 3(β) and 3(δ), we see the enhanced confinement and the interedge coupling in the SPQR.

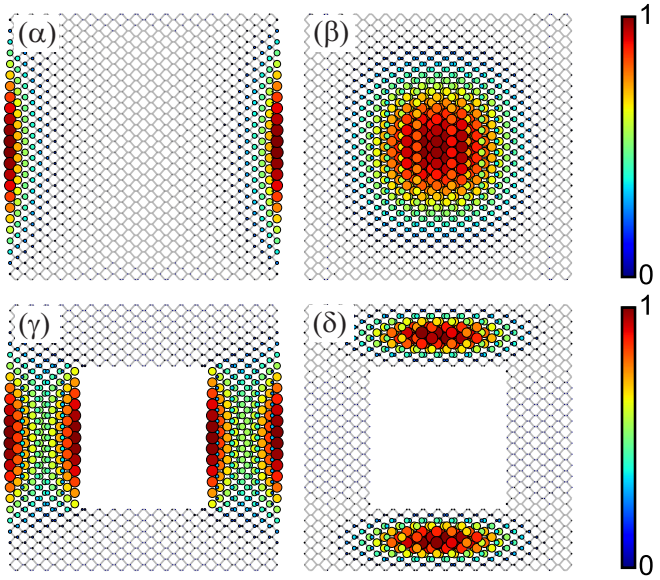

FIG. 3. Probability densities, at zero magnetic flux ($\Phi = 0$), of the lowest-energy states marked by the black dots in Fig. 2: (α) and (β) correspond to Figs. 2(c) and 2(d), respectively, (γ) and (δ) to Figs. 2(g) and 2(h), respectively.

As already shown in Fig. 2(h) [Fig. 2(f)], the bulk levels of the SPQR in the higher- (lower-) energy range in the conduction (valence) band display AB oscillations while those in the lower- (higher-) energy region in the same band show almost no oscillations, i.e., they are almost unaffected by the magnetic field. To better understand this behavior, we look at the probability densities of the corresponding energy states. Since there are many bulk energy levels involved in Fig. 2(h), we only show some of them in order to illustrate the point. Figure 4 shows the probability densities of the bulk states with given energy E and flux Φ. As can be seen in the first row, for $\Phi = 0$ the wave function of the state with $E = 0.474$ eV is mainly localized at the central region of the top and bottom arms of the ring. However, with increasing energy E, while keeping $\Phi = 0$, e.g., for $E = 1.417$ eV, the corresponding wave function is extended almost to the whole region of the ring. From the physics viewpoint, when the magnetic length $l_B = (\hbar/eB)^{1/2}$ is comparable to, or shorter than, the localization length of the wave function, the corresponding energy state will be affected by the magnetic field B. To further substantiate this viewpoint, we show in the second row of Fig. 3 how increasing the field B affects the probability densities of the energy states at $\Phi = 0$ ($B = 0$) shown in the first row. As can be seen, for lower- (higher-) energy E, the corresponding wave function is more localized (extended) and it is obviously less (more) affected by the field B. This is the main reason for our observation in Fig. 2(h) [Fig. 2(f)] that the bulk states in the higher- (lower-) energy region in the conduction (valence) band exhibit AB oscillations while those in the lower- (higher-) energy region in the same band show almost no oscillations with the field B (or the flux Φ).

B. Influence of the ring width

We now consider the influence of the ring width W on the energy spectrum of the SPQR. To this effect, in one ring we take the outer and inner sides as $L_{\rm out} = 8$ nm and $L_{\rm in} = 6$ nm long, in the other $L_{\rm out} = 8$ nm and $L_{\rm in} = 4$ nm long; this gives a width $W = 2$ nm ($W = 1$ nm) for the wider (narrower) ring. The corresponding energy spectra, as a function of the magnetic flux Φ, are shown in Figs. 5(a)–5(d), for $W = 2$ nm, and in Figs. 5(e)–5(h) for $W = 1$ nm. As can be seen, with decreasing W the bulk energy levels exhibit more regular AB oscillations. This can be understood by invoking an ideal circular ring ($W \to 0$) whose energy spectrum is given by

$$E(l,\Phi) = \frac{\hbar^2}{2m^* R^2}(l - \Phi/\Phi_0)^2. \qquad (3)$$

Here, l is the angular quantum number which takes integer values, m^* is the electron effective mass, and R the radius of the ring. Equation (3) shows that the energy spectrum of the ideal ring exhibits perfect periodic AB oscillations as a function of the magnetic flux Φ with period Φ_0. In contrast,

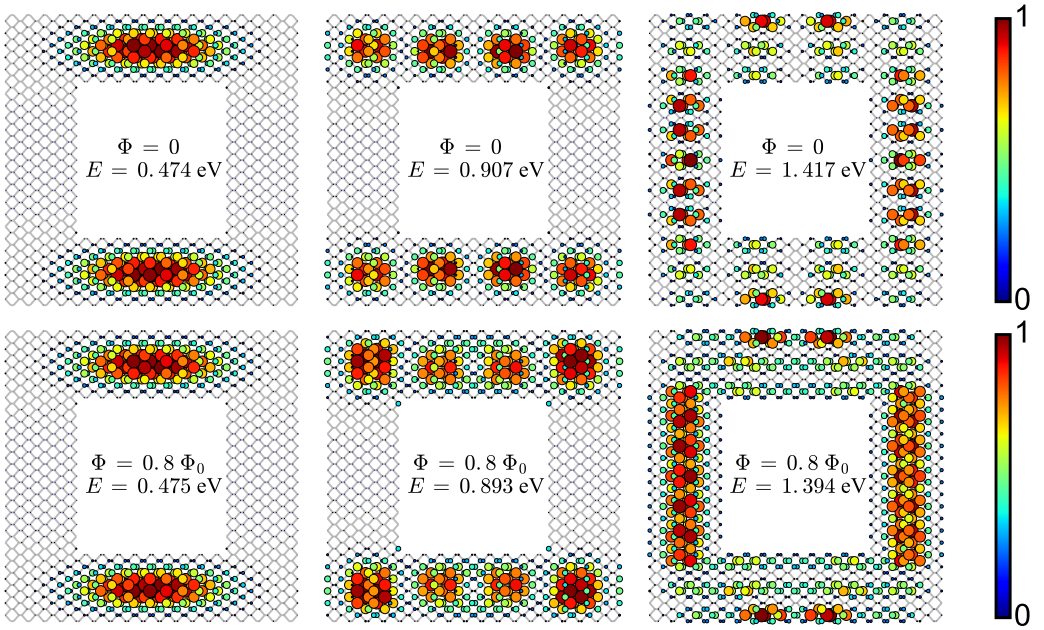

FIG. 4. Probability densities of the energy states shown in Fig. 2(h) with energy E and magnetic flux Φ, as indicated.

for the finite-width rings considered here, the period of the AB oscillations is not Φ_0 but close to $0.5\Phi_0$. Our numerical results indicate that upon further decreasing W the period becomes much closer to $0.5\Phi_0$. Note that the angular quantum number l is well defined in an ideal ring (i.e., its energy levels with different l's are crossing each other), but is not a good quantum number in a square ring due to the lack of perfect circular symmetry (which is broken by the square ring boundaries). In

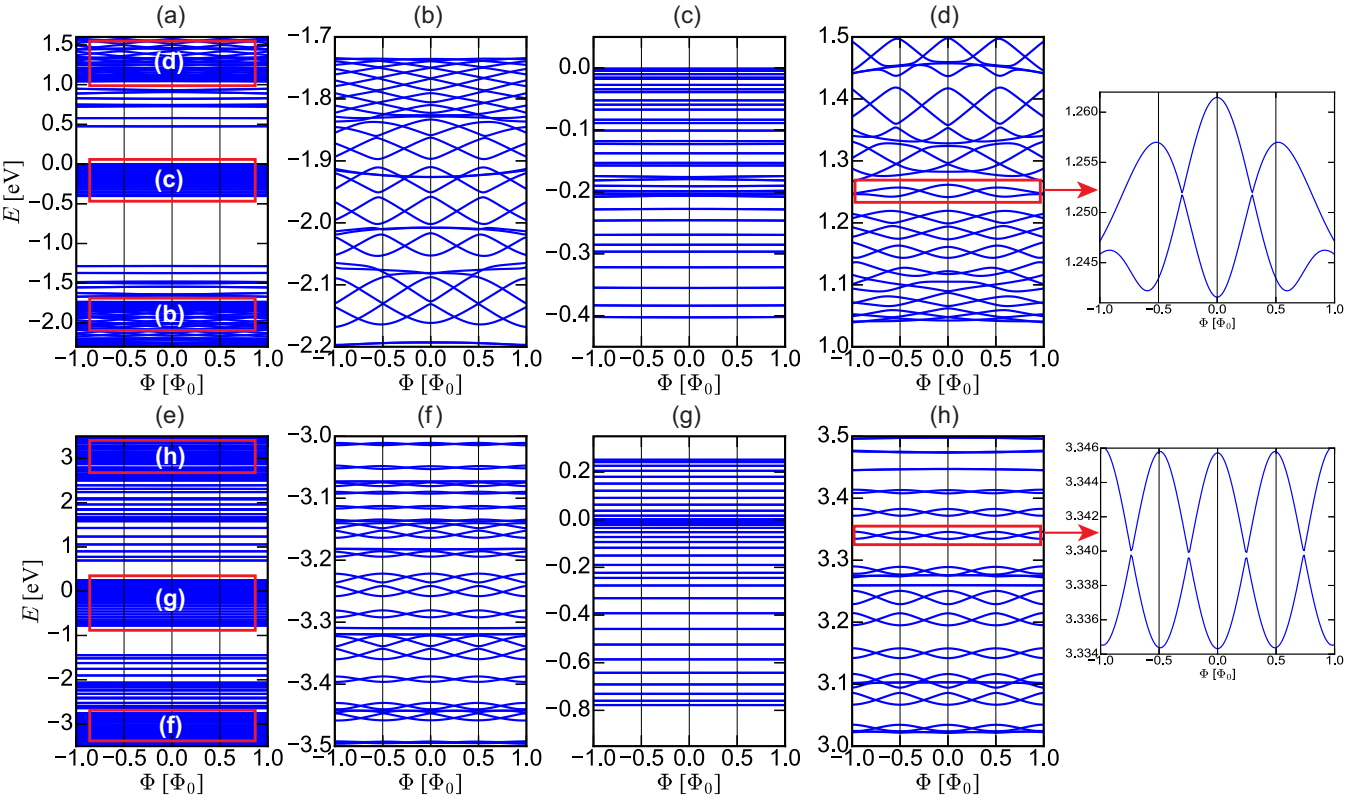

FIG. 5. Energy spectrum of a SPQR, with armchair and zigzag edges, as a function of the magnetic flux. The ring width is $W = 2$ nm in the upper panels and $W = 1$ nm in the lower ones. The outer sides are $L_{\text{out}} = 8$ nm long for both rings. The marking of the panels is the same as in Fig. 2.

the SPQR, this symmetry breaking leads to the interaction of oscillating energy levels and thus anticrossings between these levels. Such anticrossings account for halving the period of the AB oscillations in a SPQR (close to $0.5\Phi_0$).

Another interesting observation is that there also exist some nonoscillating energy levels embedded in those oscillating ones. These two distinctive sets of energy levels are induced by different confinement effects along the x (armchair) and y (zigzag) directions. Fundamentally, this is because the band anisotropy of bulk phosphorene gives rise to different electron/hole effective masses along the armchair and zigzag directions [28]. We also observe that the edge-state levels in the narrower ring are almost unaffected by the magnetic field B. This is counterintuitive because, according to what is mentioned above, the edge states in a narrow ring should be more delocalized due to the interedge coupling and therefore should be more affected by the field B. However, the fact that in narrow rings the geometric confinement is stronger than the magnetic one leads to the counterintuitive observation. In addition, due to this strong geometric confinement, the bulk energy levels are grouped into many subbands separated by energy gaps.

C. Influence of electrostatic potentials

To study the effect of electrostatic potentials on the energy spectrum of a SPQR, we consider two configurations: One is to apply a uniform in-plane electric field to the SPQR and the other to apply an asymmetric side gating to it. The influence of an in-plane field on the AB effect was earlier studied experimentally in a normal metal ring (Sb loop) [40] by placing it between two capacitor probes. It was shown that such a field can be used to tune the AB oscillations in the magnetoresistance of the loop. More recently, the influence of an asymmetric side gating on the AB effect was experimentally studied in a graphene circular ring [13] with two different side voltages applied to its arms (sides). It was found that a π phase change can be induced in the AB oscillations.

As mentioned previously, in a SPQR only bulk states in the conduction and valence bands exhibit the AB oscillations while edge states in the bulk band gap show no such oscillations. In Fig. 6 we show the effects of an in-plane electric field F_x and of a side-gating potential V_y on the oscillating energy levels in the conduction band of a SPQR with outer and inner side lengths $L_{\text{out}} = 8$ nm and $L_{\text{in}} = 4$ nm. The field F_x is applied along the armchair direction of the SPQR and the potential V_y is applied asymmetrically to its upper and lower arms [see Fig. 1(b)]. These configurations are similar to those used in Refs. [13,40]. As can be seen by comparing Figs. 6(a), 6(b), and 6(c), the AB oscillations of the energy levels become weaker and some of them even disappear in the presence of the field F_x or the potential V_y. To understand the weakened oscillations in these energy levels, we may again look at the probability densities of the corresponding energy states, as

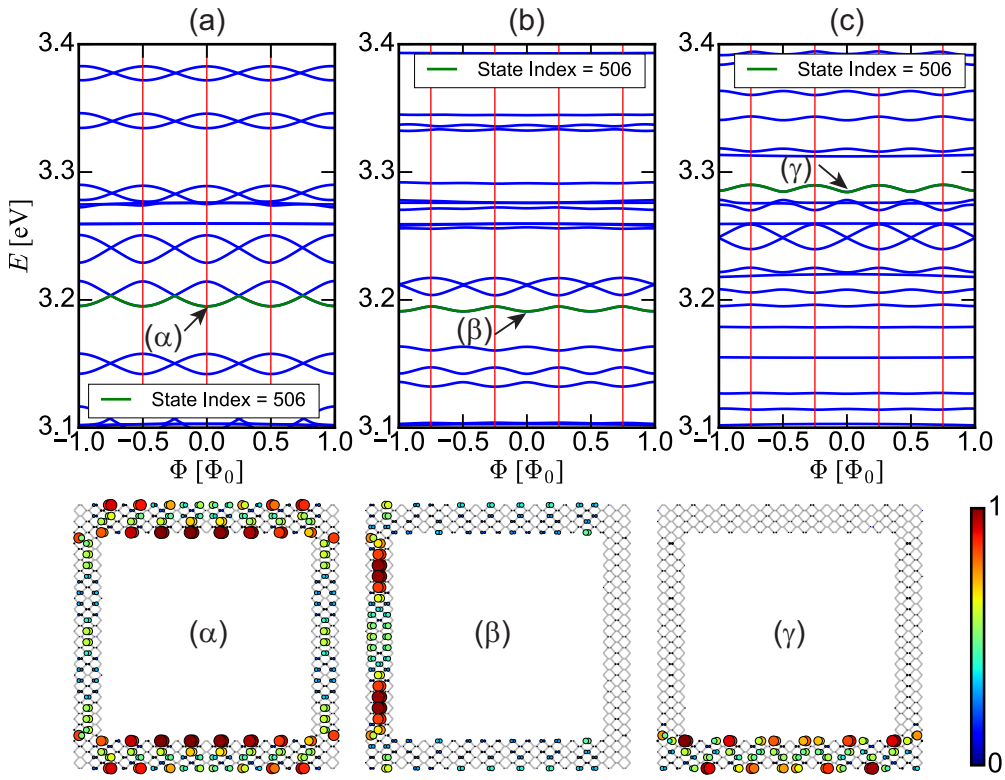

FIG. 6. Energy spectrum [(a)–(c)] and wave functions [(α)–(γ)] of a SPQR, with outer (inner) side length $L_{\text{out}} = 8$ nm ($L_{\text{in}} = 6$ nm) and with armchair and zigzag edges, as a function of the magnetic flux, in the absence and presence of an in-plane electric field F_x or an asymmetric side-gating potential V_y. (a) and (α) are for $F_x = 0$ and $V_y = 0$, (b) and (β) for $F_x = 0.05$ V/nm and $V_y = 0$, and (c) and (γ) for $F_x = 0$ and $V_y = 0.25$ V. The energy levels indicated by the green curves have the same state index of 506 in the whole energy spectrum, as indicated in (a)–(c).

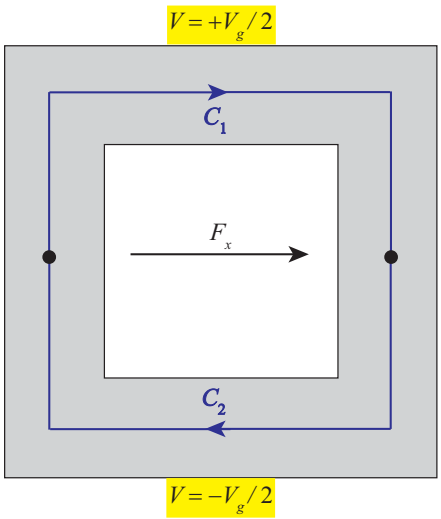

FIG. 7. Schematic plot of a model square ring in the presence of an electric field F_x or side-gating potentials $\pm V_g/2$. Here, C_1,C_2 denote two particle's traveling paths that are separated by two black dots, as indicated.

those shown in Fig. 4. The probability densities corresponding to the points indicated by arrows in Figs. 6(a), 6(b), and 6(c) are shown in Figs. 6(α), 6(β), and 6(γ), respectively. As can be seen, the field F_x or potential V_y tends to further localize the bulk states, thereby making them difficult to be affected by the magnetic field, and thus leads to weaker oscillations in the energy levels. Another interesting result is that there is no phase shift in the AB oscillations of the energy levels when the field or potential is present. To show this result clearly, we choose typical energy levels indicated by the green curves in Figs. 6(a)–6(c). These energy levels have the same state index of 506 in the whole energy spectrum. It is clear that there is no phase shift between them, i.e., their local energy maximum and minimum positions are not changed in the presence of the electric field or gate potential. Below, we give a physical explanation of this zero phase shift.

The AB effect is the modulation of the phase of the particle wave function by electromagnetic potentials. The extra phase acquired by the particle wave function due to an electric potential V is given by [3] $\varphi = (q/\hbar)\int(V/v)dl$, where q is the charge of the particle and v its velocity. We consider a model square ring in the presence of an electric field F_x or side-gating potentials $\pm V_g/2$, as shown in Fig. 7. Note the model ring is in a closed type, i.e., it has no leads, which is as that considered in the present work. The relative phase change of the particle's traveling paths $C1$ and $C2$ can be written as $\Delta\varphi = \varphi_1 + \varphi_2 = (q/\hbar)\int_C(V/v)dl$, with $C = C_1 + C_2$ and the subscripts 1 and 2 denoting the two traveling paths. Since the velocity is independent of the particle's traveling path, we obtain $\Delta\varphi = 0$ after performing an integral over the closed loop C formed by the traveling paths C_1 and C_2. This accounts for why there is no phase shift in the AB oscillations in a closed ring (without leads).

Our numerical results also indicate that for the field F_y (applied along the zigzag direction) or the potential V_x (applied asymmetrically to the left and right arms), a similar effect, i.e., reduced amplitude and no phase shift of the AB oscillations, can also be observed in a SPQR. Moreover, the amplitude of the AB oscillations in a SPQR can be effectively tuned by varying the field F_x or F_y, as shown in Fig. 8. Since the potential V_x (V_y) has a similar effect on the AB oscillations as the field F_x (F_y), we only show the results for the field case in this figure, where the left (right) panels of Fig. 8 are for the field F_x (F_y) along the armchair (zigzag) direction. In the numerical calculation, the outer and inner side lengths are taken as $L_{\rm out} = 8$ nm and $L_{\rm in} = 6$ nm, and the amplitude is defined as $\Delta E = \max(E_n) - \min(E_n)$ with E_n being the energy level of the nth eigenstate. As the top parts in both panels show, the energy levels in the SPQR depend sensitively on F_x (F_y), and these levels are coupled together, leading to anticrossings in the energy spectrum. In particular, more anticrossings are observed for F_y than for F_x. This is mainly

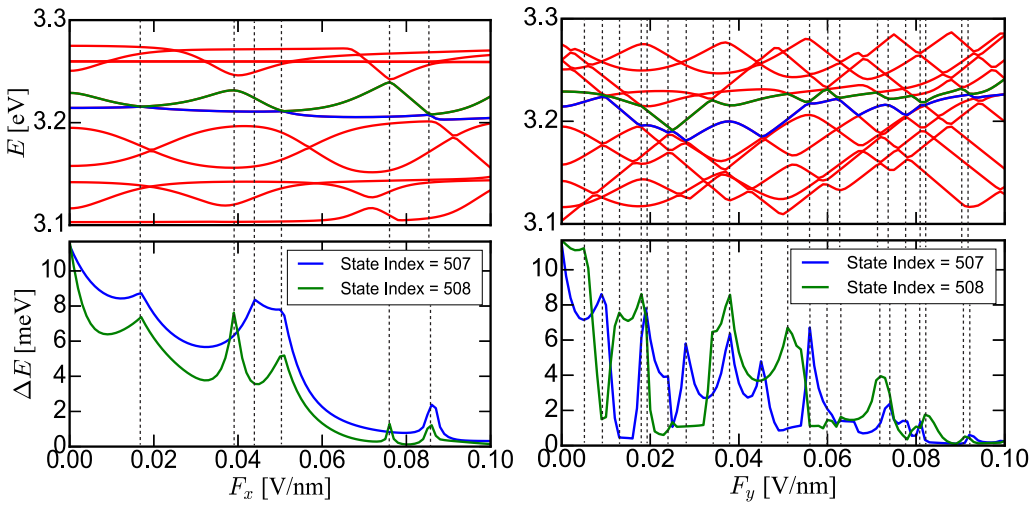

FIG. 8. Energy spectrum (E) and AB-oscillation amplitude (ΔE) of a SPQR, with outer (inner) side length $L_{\rm out} = 8$ nm ($L_{\rm in} = 6$ nm) and with armchair and zigzag edges, as a function of the field F_x along the armchair direction (left panels) or of the field F_y along the zigzag direction (right panels). Only results for two energy levels are shown for the amplitude and their state indices are indicated in the bottom panels. The vertical thin black dashed lines indicate the positions of the amplitude peaks.

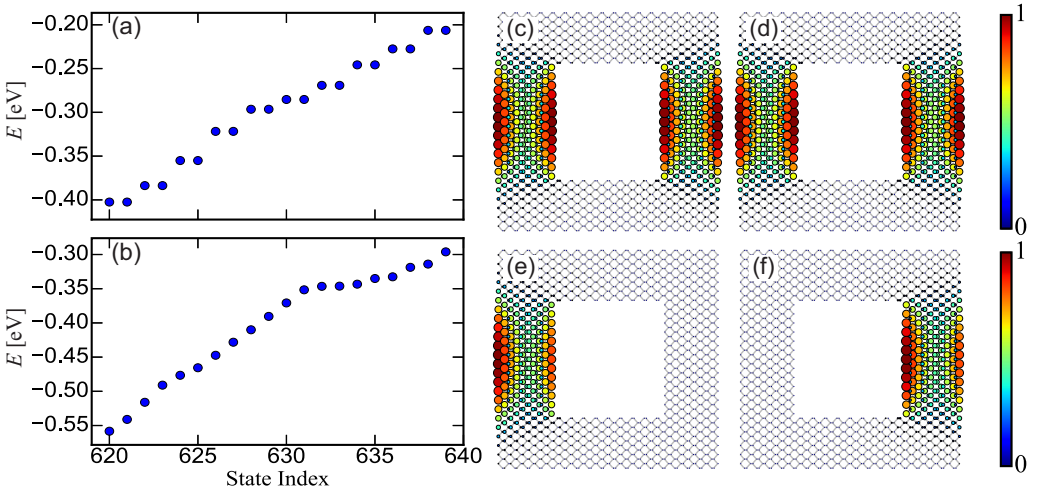

FIG. 9. (a) and (b) Energy of a few lowest edge states, vs state index, in a SPQR of inner (outer) side length $L_{\text{in}} = 4$ nm ($L_{\text{out}} = 8$ nm), with armchair and zigzag edges, at $\Phi = 0$, for (a) $F_x = 0$ and (b) $F_x = 0.05$ V/nm. (c) and (d) show the probability densities of the two lowest edge states in (a) while (e) and (f) show those of the two lowest states in (b).

due to the anisotropic energy spectrum of phosphorene, i.e., different energy dispersions exist along the armchair and zigzag directions. To clearly show how F_x or F_y affects the amplitude of the AB oscillations in the SPQR, we choose only two energy levels that exhibit AB oscillations. Their state indices are 507 and 508 in the whole energy spectrum, as indicated in the lower panels. Notice that in both cases the amplitude (ΔE) oscillates as a function of the field, F_x or F_y, with an overall decreasing trend interrupted by some oscillatory behavior. This behavior of the amplitude is induced by the anticrossings of these energy levels. For instance, the energy levels indicated by the green and blue curves have anticrossings not only with each other but also with neighboring levels, and the positions of amplitude peaks correspond to the field values at the anticrossing points. Consequently, the number of the amplitude peaks is larger for F_y than for F_x. The overall decreasing trend of the amplitude is due to the field- or potential-enhanced localization of electronic states.

Furthermore, we find that the edge-state levels are twofold degenerate in the absence of the electric field or side-gating potential. The degeneracy is lifted for nonzero field or potential because the spatial symmetry is broken by either of them. In Fig. 9(a) we show the degeneracy of the edge levels at zero field $F_x = 0$ and in Fig. 9(b) their lifting at nonzero field $F_x = 0.05$ V/nm. Similar results are obtained for the field F_y. To understand the lifting of this degeneracy, we contrast the probability densities of edge states for $F_x = 0$ and $F_x = 0.05$ V/nm. In Figs. 9(c)–9(f), we show the effect of $\boldsymbol{F_x}$ on the probability densities of the two lowest edge states in Fig. 9(a): Figs. 9(c) and 9(d) are for $F_x = 0$, and Figs. 9(e) and 9(f) for $F_x = 0.05$ V/nm. As can be seen, the two lowest edge states have the same probability densities for $F_x = 0$ and both of them are symmetrically localized at the inner and outer zigzag boundaries of the ring [see Figs. 9(c) and 9(d)], which implies that they are degenerate for $F_x = 0$. However, this degeneracy is broken for $F_x = 0.05$ V/nm and the two states localize only on the left or right zigzag arms of the ring [see Figs. 9(e) and 9(f)]. The side-gating potential V_x or V_y has a similar effect on these edge states and their probability densities.

D. Influence of geometry, contrast with graphene, and conventional 2DEG

So far we presented results only for square phosphorene rings. One may wonder (i) what changes occur in the period, if any, when other ring shapes are considered, and (ii) how the results for SPQRs compare with square rings made of graphene or conventional two-dimensional electron gas (2DEG).

Regarding (i), we also studied circular, nanometer-sized phosphorene rings. Though we do not show the results, we can affirm that the period of the AB oscillations in circular phosphorene quantum rings is the same as in SPQRs, i.e., it is close to $0.5\Phi_0$, and when the rings are placed in a field (F_x, F_y) or side gated by a potential (V_x, V_y), the amplitude of the AB oscillations is reduced. As for (ii), the period for square graphene quantum rings, with armchair and zigzag edges, is again close to $0.5\Phi_0$. The same holds for quantum rings made of conventional 2DEG (see Ref. [9]), where a period $0.5\Phi_0$ was found. This is not surprising as the mechanism for reducing the period from Φ_0 to $0.5\Phi_0$ is in all cases the interaction (i.e., coupling) between different energy levels (or modes) that lead to anticrossings in the energy spectrum as most clearly shown in the enlarged red-framed windows of Figs. 5(d) and 5(h). The intermode coupling is mainly caused by the symmetry breaking induced by the ring boundaries, i.e., anisotropic (zigzag and armchair) boundaries. Before closing we point out that the AB oscillations predicted here might be experimentally observed by optical means, e.g., through measuring magnetic-field-dependent absorption/emission spectra. Such optical means have indeed been used to detect the AB effect in semiconductor rings [7] and carbon nanotubes [41].

IV. CONCLUDING REMARKS

Using the TB method we have investigated the AB effect in nanometer-sized SPQRs with armchair and zigzag edges. The energy spectra and wave functions of such SPQRs were

obtained as a function of the magnetic flux threading the rings. We found that, compared to SPQDs, SPQRs show enhanced confinement and interedge coupling which have a large impact on the energy spectra and wave functions. From the probability densities of the electronic states, we can clearly distinguish between bulk and edge states that depend differently on the magnetic flux Φ: The bulk energy levels change periodically with Φ while the edge energy levels are almost unaffected by it. As a result, AB oscillations are observed in the bulk energy spectra of SPQRs in the conduction (valance) bulk states in the higher- (lower-) energy region but not in the edge energy spectra of SPQRs.

We further examined the effects of the ring width, of an in-plane electric field, and of an asymmetric side-gating potential on the energy spectra and the wave functions of SPQRs. We found that (1) as the ring width decreases, the AB oscillations become more regular but their period is not the magnetic flux quantum Φ_0 of the ideal ring but close to $\Phi_0/2$ due to the interaction between different energy levels or modes that lead to anticrossings; (2) in the presence of an electric field or a side-gating potential, the amplitude of the AB oscillations is reduced, compared to that in their absence; and (3) the amplitude can be effectively tuned by the field or potential and exhibits an anisotropic behavior for different field directions or side-gating configurations. We analyzed and discussed the results using the wave functions of bulk and edge states in SPQRs.

ACKNOWLEDGMENTS

This work was financially supported by the Chinese Academy of Sciences, the Flemish Science Foundation (FWO-Vl), and by the Canadian NSERC Grant No. OGP0121756 (P.V.).

[1] T. Ihn, *Semiconductor Nanostructures* (Oxford University Press, Oxford, UK, 2010).
[2] V. M. Fomin, *Physics of Quantum Rings* (Springer, Berlin, 2014).
[3] Y. Aharonov and D. Bohm, Phys. Rev. **115**, 485 (1959).
[4] M. Buttiker, Y. Imry, and R. Landauer, Phys. Lett. A **96**, 365 (1983).
[5] W. Rabaud, L. Saminadayar, D. Mailly, K. Hasselbach, A. Benoît, and B. Etienne, Phys. Rev. Lett. **86**, 3124 (2001).
[6] A. Fuhrer, S. Luscher, T. Ihn, T. Heinzel, K. Ensslin, W. Wegscheider, and M. Bichler, Nature (London) **413**, 822 (2001).
[7] M. Bayer, M. Korkusinski, P. Hawrylak, T. Gutbrod, M. Michel, and A. Forchel, Phys. Rev. Lett. **90**, 186801 (2003).
[8] N. A. J. M. Kleemans, I. M. A. Bominaar-Silkens, V. M. Fomin, V. N. Gladilin, D. Granados, A. G. Taboada, J. M. Garcia, P. Offermans, U. Zeitler, P. C. M. Christianen, J. C. Maan, J. T. Devreese, and P. M. Koenraad, Phys. Rev. Lett. **99**, 146808 (2007).
[9] L. Wendler, V. M. Fomin, and A. A. Krokhin, Phys. Rev. B **50**, 4642 (1994).
[10] T. Chakraborty and P. Pietiläinen, Phys. Rev. B **52**, 1932 (1995).
[11] J. Splettstoesser, M. Governale, and U. Zülicke, Phys. Rev. B **68**, 165341 (2003).
[12] S. Russo, J. B. Oostinga, D. Wehenkel, H. B. Heersche, S. S. Sobhani, L. M. K. Vandersypen, and A. F. Morpurgo, Phys. Rev. B **77**, 085413 (2008).
[13] M. Huefner, F. Molitor, A. Jacobsen, A. Pioda, C. Stampfer, K. Ensslin, and T. Ihn, New. J. Phys. **12**, 043054 (2010).
[14] D. Smirnov, H. Schmidt, and R. J. Haug, Appl. Phys. Lett. **100**, 203114 (2012).
[15] D. Cabosart, S. Faniel, F. Martins, B. Brun, A. Felten, V. Bayot, and B. Hackens, Phys. Rev. B **90**, 205433 (2014).
[16] P. Recher, B. Trauzettel, A. Rycerz, Ya. M. Blanter, C. W. J. Beenakker, and A. F. Morpurgo, Phys. Rev. B **76**, 235404 (2007).
[17] D. S. L. Abergel, V. M. Apalkov, and T. Chakraborty, Phys. Rev. B **78**, 193405 (2008).
[18] D. A. Bahamon, A. L. C. Pereira, and P. A. Schulz, Phys. Rev. B **79**, 125414 (2009).
[19] M. Zarenia, J. M. Pereira, A. Chaves, F. M. Peeters, and G. A. Farias, Phys. Rev. B **81**, 045431 (2010).
[20] P. Potasz, A. D. Güçlü, O. Voznyy, J. A. Folk, and P. Hawrylak, Phys. Rev. B **83**, 174441 (2011).
[21] I. Romanovsky, C. Yannouleas, and U. Landman, Phys. Rev. B **85**, 165434 (2012).
[22] J. Schelter, P. Recher, and B. Trauzettel, Solid State Commun. **152**, 1411 (2012).
[23] L. Li, Y. Yu, G. J. Ye, Q. Ge, X. Ou, H. Wu, D. Feng, X. H. Chen, and Y. Zhang, Nat. Nanotechnol. **9**, 372 (2014).
[24] H. Liu, A. T. Neal, Z. Zhu, Z. Luo, X. Xu, D. Tomanek, and P. D. Ye, ACS Nano **8**, 4033 (2014).
[25] K. S. Novoselov, A. K. Geim, S. V. Morozov, D. Jiang, M. I. Katsnelson, I. V. Grigorieva, S. V. Dubonos, and A. A. Firsov, Nature (London) **438**, 197 (2005).
[26] Q. H. Wang, K. Kalantar-Zadeh, A. Kis, J. N. Coleman, and M. S. Strano, Nat. Nanotechnol. **7**, 699 (2012).
[27] S. Das, W. Zhang, M. Demarteau, A. Hoffmann, M. Dubey, and A. Roelofs, Nano Lett. **14**, 5733 (2014).
[28] J. Qiao, X. Kong, Z. X. Hu, F. Yang, and W. Ji, Nat. Commun. **5**, 4475 (2014).
[29] F. Xia, H. Wang, and Y. Jia, Nat. Commun. **5**, 4458 (2014).
[30] S. Yuan, A. N. Rudenko, and M. I. Katsnelson, Phys. Rev. B **91**, 115436 (2015).
[31] X. Zhang, H. Xie, Z. Liu, C. Tan, Z. Luo, H. Li, J. Lin, L. Sun, W. Chen, Z. Xu, L. Xie, W. Huang, and H. Zhang, Angew. Chem. Int. Ed. **54**, 3653 (2015).
[32] Z. Sun, H. Xie, S. Tang, X. F. Yu, Z. Guo, J. Shao, H. Zhang, H. Huang, H. Wang, and P. K. Chu, Angew. Chem. Int. Ed. **127**, 11688 (2015).
[33] R. Zhang, X. Y. Zhou, D. Zhang, W. K. Lou, F. Zhai, and K. Chang, 2D Mater. **2**, 045012 (2015).
[34] X. Niu, Y. Li, H. Shu, and J. Wang, J. Phys. Chem. Lett. **7**, 370 (2016).
[35] L. L. Li, D. Moldovan, W. Xu, and F. M. Peeters, Nanotechnology **28**, 085702 (2017).
[36] A. N. Rudenko and M. I. Katsnelson, Phys. Rev. B **89**, 201408(R) (2014).

[37] V. Wang, Y. C. Liu, Y. Kawazoe, and W. T. Geng, J. Phys. Chem. Lett. **6**, 4876 (2015).

[38] M. Ezawa, New J. Phys. **16**, 115004 (2014).

[39] D. Moldovan and F. M. Peeters, PYBINDING *v0.8.0: A Python Package for Tight-Binding Calculations*, http://dx.doi.org/10.5281/zenodo.56818.

[40] S. Washburn, H. Schmid, D. Kern, and R. A. Webb, Phys. Rev. Lett. **59**, 1791 (1987).

[41] S. Zaric, G. N. Ostojic, J. Kono, J. Shaver, V. C. Moore, and M. S. Strano, R. H. Hauge, R. E. Smalley, and X. Wei, Science **304**, 1129 (2004).